Check for updates

Electrochemistry | Hot Paper |

Electrolyte Structure of Lithium Polysulfides with Anti-Reductive Solvent Shells for Practical Lithium–Sulfur Batteries

Xue-Qiang Zhang[+], Qi Jin[+], Yi-Ling Nan[+], Li-Peng Hou, Bo-Quan Li, Xiang Chen, Zhe-Hui Jin, Xi-Tian Zhang, Jia-Qi Huang, and Qiang Zhang*

Abstract: The lithium–sulfur (Li–S) battery is regarded as a promising secondary battery. However, constant parasitic reactions between the Li anode and soluble polysulfide (PS) intermediates significantly deteriorate the working Li anode. The rational design to inhibit the parasitic reactions is plagued by the inability to understand and regulate the electrolyte structure of PSs. Herein, the electrolyte structure of PSs with anti-reductive solvent shells was unveiled by molecular dynamics simulations and nuclear magnetic resonance. The reduction resistance of the solvent shell is proven to be a key reason for the decreased reactivity of PSs towards Li. With isopropyl ether (DIPE) as a cosolvent, DIPE molecules tend to distribute in the outer solvent shell due to poor solvating power. Furthermore, DIPE is more stable than conventional ether solvents against Li metal. The reactivity of PSs is suppressed by encapsulating PSs into anti-reductive solvent shells. Consequently, the cycling performance of working Li–S batteries was significantly improved and a pouch cell of 300 Wh kg^{-1} was demonstrated. The fundamental understanding in this work provides an unprecedented ground to understand the electrolyte structure of PSs and the rational electrolyte design in Li–S batteries.

Introduction

The pursuit of sustainable society and carbon neutrality by utilizing renewable but intermittent energy, such as wind and solar energy, requires long-lived, stable and low-cost energy storage systems.[1] Besides, the vision for wireless life also stimulates the demand for portable electronics with high specific energy and long durability. Therefore, rechargeable batteries based on the energy storage mechanism of conversion reactions beyond the intercalation reactions of Li-ion batteries are reviving.[2,3] Lithium–sulfur (Li–S) battery emerges as a promising candidate due to the theoretically

high specific energy and low material cost.[4] The specific energy of practical Li–S batteries at a cell level is also attractive, as it can be over 500 Wh kg^{-1} when using S/carbon composite cathode.[5] In contrast to the intercalation mechanism of Li-ion batteries, S/carbon cathode falls into a solid–liquid–solid conversion mechanism.[4] Soluble Li polysulfide (PS) intermediates, e.g., Li$_2$S$_{4-8}$, are generated from solid S$_8$ at the first plateau and then are reductively transformed into solid Li$_2$S$_2$ or Li$_2$S at the second plateau during a discharge process.[4] Owing to facile charge transfer and the redox mediation to solid products, dissolved PSs facilitate the high specific capacity and high discharge voltage of S/carbon cathode compared with other types of S cathode.[6–8] Therefore, the solution-mediated stage with dissolved PSs is pivotal for fully utilizing high specific energy of Li–S batteries with S/carbon composite cathode.

However, dissolved PSs induce severe challenges for stable Li metal anode despite their key role in promoting the conversion of S. Li metal is highly reductive and the parasitic reactions between Li and PSs are inevitable. Generally, the consumption of Li metal anode by the parasitic reactions and its corresponding contribution to the decay of a battery are concealed thanks to the sufficient supply of fresh Li,[9] when employing mild conditions for fundamental researches, including much excessive Li (>500 μm), flooded electrolytes (>20.0 μL mg$_S^{-1}$), and low S loading (<2.0 mg$_S$ cm^{-2}).[10] However, practical conditions with limited Li (<50 μm), lean electrolytes (<3.0 μL mg$_S^{-1}$), and high S loading (>4.0 mg$_S$ cm^{-2}) are necessary for the aim of specific energy over 500 Wh kg^{-1}.[11] Limited Li can be rapidly depleted by the parasitic reactions when negative/positive (N/P) capacity ratio decreases from 30 to 1.6, rendering a bottleneck of long-cycling practical Li–S batteries.[12,13] Furthermore, a non-uniform Li deposition, namely Li filaments or dendrites, provides a large reactive surface area exposed to PSs.[14] The

[*] X.-Q. Zhang,[+] L.-P. Hou, Dr. X. Chen, Prof. Q. Zhang
Beijing Key Laboratory of Green Chemical Reaction Engineering and Technology, Department of Chemical Engineering
Tsinghua University
Beijing 100084 (P. R. China)
E-mail: zhang-qiang@mails.tsinghua.edu.cn

Q. Jin,[+] Prof. X.-T. Zhang
Key Laboratory for Photonic and Electronic Bandgap Materials
Ministry of Education, School of Physics and Electronic Engineering
Harbin Normal University
Harbin 150025 (P. R. China)

Y.-L. Nan,[+] Prof. Z.-H. Jin
School of Mining and Petroleum Engineering, Department of Civil and Environmental Engineering, University of Alberta
Edmonton ABT6G 1H9 (Canada)

Dr. B.-Q. Li, Prof. J.-Q. Huang
Advanced Research Institute of Multidisciplinary Science
Beijing Institute of Technology
Beijing 100081 (P. R. China)

[+] These authors contributed equally to this work.

Supporting information and the ORCID identification number(s) for the author(s) of this article can be found under:
https://doi.org/10.1002/anie.202103470.

parasitic reactions between Li anode and dissolved PSs are then accelerated. Therefore, suppressing the parasitic reactions with PSs to protect Li metal anode is imperative, especially for practical Li–S batteries.

Compared with physical hosts/barriers[15–17] and chemical catalysis/adsorption[18–21] to confine the diffusion or promote the transformation of PSs, electrolyte design, especially the fundamental understanding of electrolyte structure, provides an intrinsic and rational method to inhibit the parasitic reactions.[22–24] The electrolyte structure in Li–S batteries is unprecedented due to the dissolution of PS intermediates. In common Li-ion batteries, electrolyte structure only focuses on solvents and Li salts because no electrode redox product dissolves into electrolyte. However, in Li–S batteries, the dissolution of PSs is integrant and then the electrolyte structure of PSs is critical. Recently, sparingly solvating electrolytes were proposed to mitigate parasitic reactions by decreasing the solubility of PSs in electrolytes,[25] such as solvated ionic liquids,[26] concentrated electrolytes,[27,28] and high carbon-to-oxygen (C/O) ratio ethers.[29–32] However, when the concentration of PSs is less than the upper limit of the solubility of sparing solvating electrolytes, all PSs are still dissolved as like in conventional electrolyte but the parasitic reactions in sparingly solvating electrolytes are mitigated, which implies that the low solubility of PSs in electrolyte is not the inherent reason of mitigating parasitic reactions. Instead, the electrolyte structure of PSs is the possible underlying reason. Furthermore, sparingly solvating electrolytes suppress the parasitic reactions at the significant cost of kinetic performance of S cathode, which is unfavorable in practical batteries.[25,33] Therefore, the fundamental understanding and rational regulation of electrolyte structures of PSs is strongly required to understand and inhibit the parasitic reactions between PSs and Li metal.

In this contribution, the electrolyte structure of PSs in typical two types of electrolyte was investigated by molecular dynamics (MD) simulations and nuclear magnetic resonance (NMR) measurements. In an electrolyte, a dissolved PS is mainly surrounded by two shells of solvent, that is inner or outer shell. The reactivity of PSs with Li was proved to highly depends on the reduction resistance of the outer solvent shells of PSs. In a conventional electrolyte, 1,3 dioxolane (DOL) with weak solvating power yet high reactivity dominates in the outer shell around PSs (Figure 1a). In an electrolyte with isopropyl ether (DIPE) as a cosolvent, DIPE molecules tend to distribute in the outer solvent shell around PSs due to poor solvating power and the inner shell is only composed of DOL and dimethoxyethane (DME, Figure 1b). DIPE molecule has
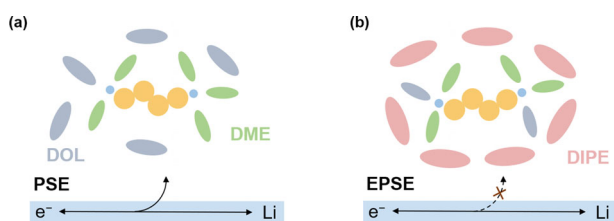
a higher stability than conventional ether solvents against Li metal and thus the reduction resistance of the outer shell is improved. Consequently, PSs were encapsulated into anti-reductive solvent shells to mitigate the parasitic reactions. Meanwhile, the dissolution of PSs is ensured by the conventional ether solvents in the inner shell, facilitating the kinetic performance of S cathode. Therefore, a working Li–S battery under practical conditions delivered 120 cycles compared to 62 cycles in conventional ether electrolytes. Moreover, a pouch cell (1.6 Ah) with a specific energy of 300 Wh kg^{-1} was achieved to evaluate the potential under a practical scene.

Results and Discussion

Electrolyte structure of PSs

The conventional ether electrolyte, i.e., 1.0 M Li bis(trifluoromethanesulphonyl)imide (LiTFSI) in DOL/DME (1:1, by vol., denoted as PSE), is the state-of-the-art electrolyte in Li–S batteries. The parasitic reactions between Li and PSs are notorious owing to a relatively high solubility (ca. 0.5 M Li_2S_8) of PSs in the conventional ether electrolyte.[6,29] In order to investigate the electrolyte structure of different types of dissolved PSs, a low concentration (2.5 mM) of PS was employed to ensure a thorough dissolution. Moreover, the electrolyte structures of typical PSs, such as S_4^{2-}, S_6^{2-}, and S_8^{2-}, were, respectively studied by MD simulations to provide a full view. S_4^{2-} was then selected as an example for a detailed illustration due to similar electrolyte structures of dissolved PSs.

In the conventional ether electrolyte, S_4^{2-} interacts with Li^+ strongly due to the shortest distance (0.18 nm) from S_4^{2-} center as in previous reports,[34,35] although Li_2S_4 is dissolved into the electrolyte. The terminal S atom plays a vital role in interacting with Li^+.[36] Meanwhile, Li^+ is solvated by solvents, such as DOL and DME, forming solvation sheaths around Li^+ (Figure S3).[37] Due to the strong binding, S_4^{2-} is also involved in the solvation sheath of Li^+ according to the range of classical primary solvation sheath (≈ 0.2 nm, Figure S3).[38] Objectively, from the view of S_4^{2-}, S_4^{2-} is surrounded by the solvent shells. Solvent shells are composed of the solvents in the solvation sheath of Li^+. According to radial distribution functions (RDFs) around S_4^{2-} (Figure 2a), there are two concentric solvent shells with their peaks at 0.60 and 1.00 nm from S_4^{2-}, respectively. The two solvent shells are denoted as shell 1 and 2 outward from the center. Both solvent shells are the mixtures of DOL and DME. DME has a higher adsorption peak in the inner shell as shown in number density distribution (Figure S5), because the solvating power of DME is stronger than that of DOL.[39] On the other hand, the number density of DOL molecules in the outer shell 2 is larger than that of DME. The electrolyte structure of PSs is also in a good agreement with the empirical role of DME and DOL in the conventional ether electrolyte.[7] DME facilitates the high solubility of PSs and fast kinetical reactions. Meanwhile, DOL is unstable against Li metal and is easily decomposed to form SEI. Consequently, it is inferred that severe parasitic reactions stem from specific electrolyte
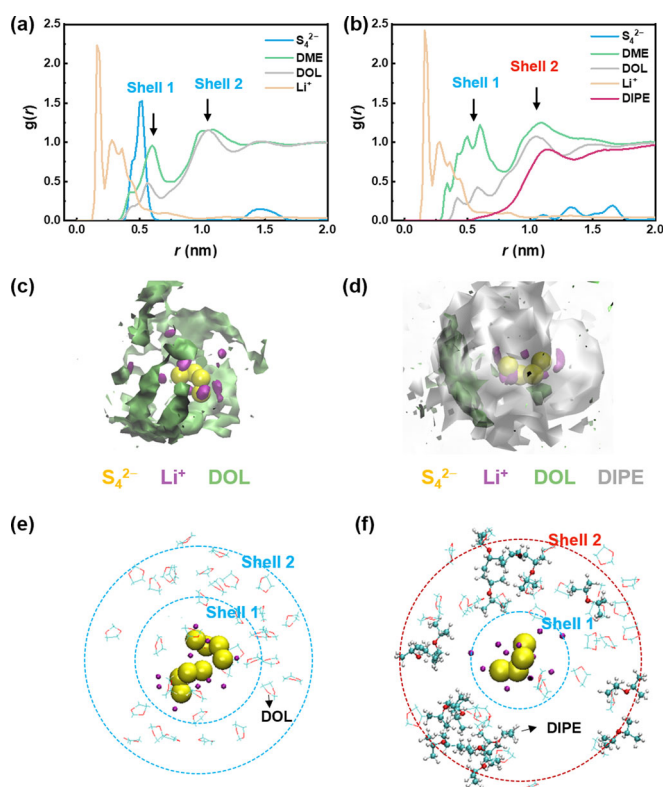

Figure 1. Scheme of electrolyte structure of PS in a) PSE and b) EPSE. Li ion and S_4^{2-} are marked by blue and yellow, respectively.

Angew. Chem. Int. Ed. **2021**, *60*, 2–9

© 2021 Wiley-VCH GmbH

www.angewandte.org

These are not the final page numbers! ↗↗

Figure 2. MD simulations of electrolyte structure. The RDFs around S_4^{2-}, $g(r)$, in a) PSE and b) EPSE. The radial distance is the center of mass (COM) distance between center (S_4^{2-}) and selected (S_4^{2-}, DME, DOL, Li^+, and DIPE) molecules. The $g(r)$ of Li^+ and S_4^{2-} is reduced by 30 and 20 times for a better comparison. Shell 1 or 2 is the shell composed of solvents, in which 1 or 2 is marked according to the distance from the COM of S_4^{2-}. SDFs of Li^+ (80 nm^{-3}) and DOL (56 nm^{-3}) in c) PSE and Li^+ (80 nm^{-3}), DOL (56 nm^{-3}), and DIPE (8 nm^{-3}) in d) EPSE around S_4^{2-}. Snapshots of the molecular distributions around S_4^{2-} in e) PSE and f) EPSE obtained from MD simulations. DME and TFSI$^-$ are omitted here for a clear comparison in (e) and (f).

structure of PSs. The outer shell with a large amount of DOL can be easily reduced, exposing PSs against Li metal to induce the parasitic reactions.

When DIPE as a co-solvent is introduced into the conventional ether electrolyte, the components of outer solvent shell are altered. DIPE has a limited solubility of PSs (< 4.0 mM) and a high solubility of LiTFSI (> 3.0 M, Figure S6) due to its high carbon/oxygen (C/O) ratio and large steric hindrance for coordinating with O atom in molecule structure.[29] Meanwhile, DIPE is also miscible with DOL and DME and displays less reactivity with Li metal than DOL (Figure S7). In this work, a moderate amount of DIPE was optimized for a compromise between the suppression of parasitic reactions and the satisfactory kinetic performance of S cathode, achieving an electrolyte composed of 1.0 M LiTFSI in DIPE/DOL/DME (3:3.5:3.5, by vol., denoted as EPSE). The ionic conductivity of EPSE (6.5 mS cm^{-1}) is high enough to support the moderate battery rate compared to PSE of 12.6 mS cm^{-1} and the sparingly solvating electrolyte of < 2 mS cm^{-1}.[30] In EPSE, S_4^{2-} is surrounded by two concentric solvent shells at 0.60 and 1.10 nm (Figure 2b). Shell 1 is only

composed of DOL and DME, which can facilitate the dissolution of PSs and then normal kinetic performance of S cathode. DIPE molecules are crowded out and become the building blocks of the outer solvent shell. The total density of DOL, especially in the outer shell, is reduced although its distribution around S_4^{2-} almost do not change after adding DIPE (Figure S5). The distribution of DME in inner shell 1 changes obviously in order to dissolve the same number of PSs after the introduction of DIPE with a low solubility of PSs (Figure S5). Furthermore, the reduction resistance of the outer shell against Li metal is enhanced due to the recruitment of DIPE which is more reductively stable than DOL, and the decreased number of DOL in the outer solvent shell. The parasitic reactions between the inside PS and Li metal are kinetically obstructed by the anti-reductive outer shell, as PS is encapsulated into an anti-reductive solvent shell containing DIPE, mitigating its exposure to fresh Li. Consequently, an encapsulating PS electrolyte (EPSE) is obtained. The spatial distribution functions (SDFs) and snapshots around S_4^{2-} display the distributions of solvents, S_4^{2-}, and Li^+ in a visualized view (Figure 2 c–f). Similar conclusions were drawn from other systems with S_6^{2-} and S_8^{2-} (Figure S1, S2).

NMR measurements were further implemented to investigate the solvation structure of Li ions in electrolytes, which can confirm the solvent shell structure of PSs predicted from MD simulations. The changes in chemical shift of ^{17}O nuclei of solvent were recorded when PSs was added into neat solvent mixtures of EPSE (Figure 3 a). The ion–dipole interaction between ethereal O in solvent and Li ions is the strong.[40] The change in electronic environment of ^{17}O nuclei indicates the variation of the ion–dipole interaction and the solvation structure of Li ions. When 0.05 M Li_2S_8 was added into EPSE, the chemical shifts of ^{17}O nuclei in DIPE, DME, and DOL apparently exhibit upfield displacements but in much different values. In particular, if the lone pair of ^{17}O are involved in ion–dipole interaction, then, the nuclear shielding increases as
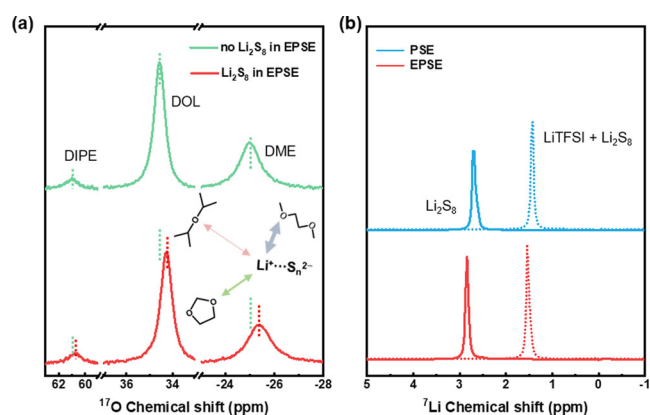

Figure 3. Nuclear magnetic resonance (NMR) spectra of ^7Li and ^{17}O in various electrolytes measured at 50 °C. a) Natural abundance ^{17}O-NMR spectra of EPSE without Li_2S_8 (green) and EPSE with 0.05 M Li_2S_8 (red). The inset is that the interaction with Li ion decreases in the order of DME, DOL and DIPE. b) ^7Li-NMR spectra of 0.10 M Li_2S_8 in PSE and EPSE (solid), and 1.0 M LiTFSI + 0.10 M Li_2S_8 in PSE and EPSE (dash). PSE and EPSE, herein, are the neat solvent mixtures without Li salt.

www.angewandte.org

These are not the final page numbers!

© 2021 Wiley-VCH GmbH

Angew. Chem. Int. Ed. **2021**, 60, 2–9

reported.[41,42] The chemical shift of ^{17}O nuclei in DME and DOL decreases from −25.0 to −25.4 ppm, 34.6 to 34.3 ppm, respectively. However, the chemical shift of ^{17}O nuclei in DIPE slightly decreases from 61.0 to 60.9 ppm. The upfield displacement of ^{17}O nuclei in DME is the most significant because the ion–dipole interaction decreases in the order of DME, DOL, and DIPE. DME displays strongest solvating power among DME, DOL, and DIPE.[39] When DIPE with a limited solubility of Li_2S_8 is introduced into electrolyte, in the primary solvation sheath, stronger ion–dipole interaction between PSs and DME and even more DME molecules in EPSE are required to ensure the full dissolution of Li_2S_8 compared with PSE. The slight upfield displacement of ^{17}O nuclei in DIPE implies that DIPE weakly interacts with Li ions and DIPE is mainly recruited into the secondary solvation sheath, resembling to the solvation structure of the diluent around Li ions in localized high-concentration electrolyte.[43]

Spontaneously, the introduction of DIPE inevitably decreases the number of solvents which can strongly interact with Li ions compared with PSE. Therefore, the deshielding of Li ions is reasonable and then the chemical shift of ^7Li was monitored (Figure 3b). In 1.20 M LiTFSI in PSE and EPSE (Figure S8), the chemical shift of ^7Li nearly has no difference because both PSE and EPSE have high solubility of LiTFSI. When 0.10 M Li_2S_8 was added into neat solvent mixtures of EPSE, the chemical shift of ^7Li increases from 2.7 to 2.8 ppm, exhibiting a downfield displacement. The deshielding of Li ions is in line with the expectations. DIPE shows sparingly solvating power to a Li ion compared with DME and DOL. DIPE is recruited into the secondary sheath of a Li ion, which decreases the amounts of DME and DOL interacting with Li ions, thus inducing the deshielding of Li ions. The downfield displacement of Li ions from 1.4 to 1.5 ppm also appears when 0.10 M Li_2S_8 was added into EPSE with 1.0 M LiTFSI. The solvation structure of Li ions from PSs is not disturbed by the addition of LiTFSI. The solvation structure of Li ions has a good agreement with MD simulation results and then solidly supports the conjecture of solvent shell structure of PSs, in which PSs are encapsulated in anti-reductive solvent shells in EPSE.

The stability of electrolytes with PSs against Li metal

The stability of bulk EPSE and PSE against Li metal was monitored to prove the effect of the encapsulation of PSs in anti-reductive solvent shells. However, solid electrolyte interphase (SEI) on Li metal anode can also be tailored to block PSs.[44] The interference from SEI is excluded aforehand (Figure S9). A Li foil formed SEI in EPSE firstly, and then it was immersed into brown PSE with 2.5 mM PSs (based on Li_2S_8). After immersion of 24 h, PSE faded into a colorless solution, implying that the SEI formed by EPSE cannot restrain the reactions between PSs and Li.

However, when a bare Li foil was directly immersed into EPSE or PSE with 2.5 mM PSs, EPSE maintains yellow for 24 h compared with the rapid discolorment of PSE (Figure 4a, b). The unchanged color of EPSE with dissolved PSs
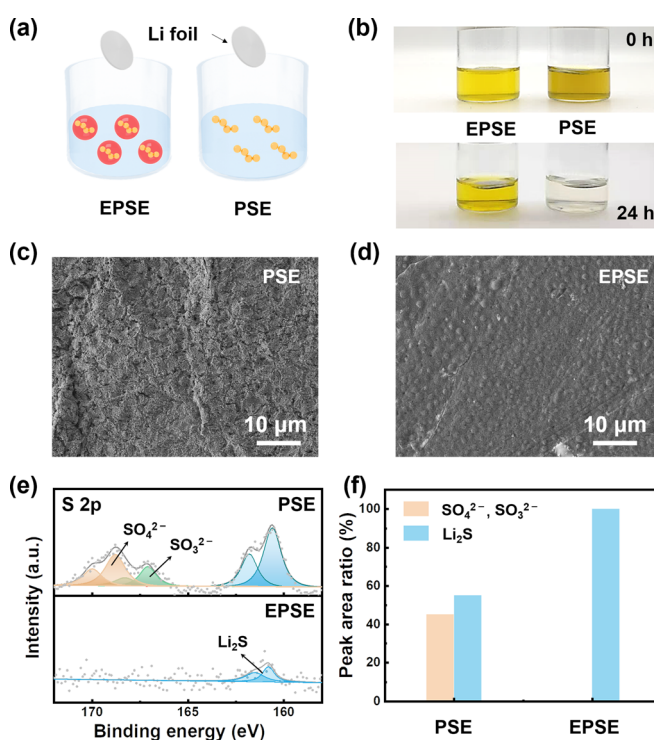

Figure 4. The stability of bulk electrolytes against Li metal. a) Schemes of direct immersion of bare Li into EPSE (left) and PSE (right). b) The optical images recording the color change of EPSE (left) and PSE (right) immersed with bare Li after 0 and 24 h. c, d) Surface morphology, e) XPS spectra of S 2p, and f) the peak area ratio of S species of bare Li after immersion in PSE and EPSE.

implies that the parasitic reactions are mitigated in EPSE. After immersion, the Li foil in PSE with PSs is corroded obviously due to the parasitic reduction reactions, exhibiting a porous and loose morphology (Figure 4c).[45] In contrast, the Li foil in EPSE is unspoiled, giving a compact morphology (Figure 4d, S10). Furthermore, the components on the surface of Li foil were detected (Figure 4e, f). The atomic concentration of S on the Li surface in EPSE is much lower than that in PSE (0.17% vs. 2.96%). Specifically, the components containing SO_4^{2-} and SO_3^{2-}, and Li_2S were detected on the surface of Li foil in PSE, in which the atomic concentration of S from Li_2S is 1.63% according to the peak area ratio (Figure 4f). However, there is only little Li_2S on the surface of Li foil in EPSE. The parasitic reactions between the encapsulated PSs in EPSE and Li metal are greatly mitigated. Consequently, the electrolyte structure of PSs is the underlying reason of mitigating parasitic reactions rather than the superficial phenomenon of low solubility of PSs.

Li–S batteries in LiNO₃-free electrolytes

The mitigation of the parasitic reactions in EPSE was assessed in Li–S full batteries and no LiNO₃ was used. The mild conditions with a thick Li anode (500 μm), flooded electrolytes (16 μL mg_S^{-1}), and a low loading S cathode (1.2 $mg_S\,cm^{-2}$) were employed in consideration of the full dissolution of PSs. When E/S ratio is 16 μL mg_S^{-1}, the

concentration of Li_2S_8 is 0.24 M theoretically and 0.14 M practically (based on 60% of theoretically specific capacity, i.e., 1000 mAh g^{-1}).[46] 0.14 M Li_2S_8 is easily dissolved into EPSE and PSE. In a Li–S cell with PSE, the specific capacity at the 1st cycle is 907 mAh g^{-1} and fades to 655 mAh g^{-1} within 5 cycles at 0.1 C (Figure 5a, S11). The CE is 85% and 59% at the 1st and 5th cycle, respectively. Much low CE and rapid failure of Li–S batteries are obtained, which are in a good agreement with the previous reports when only employing PSE.[47] However, significantly improved cycling stability and CE are achieved in EPSE. The specific capacity at the 1st cycle is 1037 mAh g^{-1} and fades to 596 mAh g^{-1} within 100 cycles. The CE is 91% at the 1st and 100th cycle although there is a fluctuation during cycles. The shuttle of PSs is mitigated based on the increased CE, which is also proved by the decreased shuttle current (Figure 5b). At varied potentiostatic voltages, the batteries in EPSE exhibit significantly reduced shuttle current by at least 17 times than that in PSE. Significantly improved CE and decreased shuttle current are in line with the expectations of the mitigated parasitic reactions in EPSE.

The morphology of Li metal anode disassembled from Li–S batteries were recorded (Figure 5c, d). The deposited Li from PSE is loose and porous after 5 cycles. However, a compact and uncorroded morphology of Li metal anode is achieved 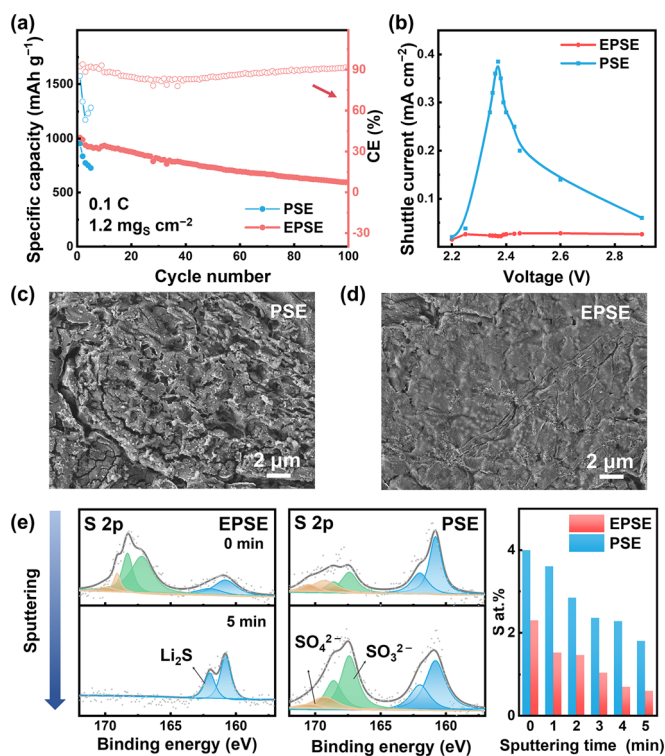in EPSE. Although the SEI formed in EPSE cannot block PSs, yet SEI contributes to improving the uniformity of Li deposition (Figure S12). There are SO_4^{2-}, SO_3^{2-}, and Li_2S on the top layer of SEI next to electrolyte in both EPSE and PSE, which decompose from TFSI$^-$ and PSs (Figure 5e, S13).[48] The bottom layer of SEI close to Li metal anode was further investigated after sputtering, providing a full view to understand the change of SEI components. Surprisingly, after 5-min sputtering, SO_4^{2-} and SO_3^{2-} components disappear and only Li_2S remains at the bottom of SEI from EPSE. However, the bottom components of SEI from PSE have little change compared with the top components. With increased sputtering time, i.e., the SEI closer to Li, the atomic concentration of S decreases. Quantitatively, the atomic concentration of S atom in SEI is lower in EPSE than PSE, 2.1% vs. 4.0% at the top, and 0.7% vs. 1.9% at the bottom. In a short conclusion, the parasitic reactions are significantly suppressed in EPSE due to the encapsulated electrolyte structure of PSs, although PSs are fully dissolved in a Li–S battery.

Li–S batteries under practical conditions in LiNO$_3$-containing electrolytes

EPSE was further evaluated in Li–S batteries under practical conditions and in pouch cells. An ultrathin Li anode (50 μm), lean electrolytes (7.5 μL mg$_S$$^{-1}$), and a high loading S cathode (4.0 mg$_S$ cm^{-2}) were included in a coin cell.[49] The amount of electrolyte is relatively higher than 5.0 μL mg$_S$$^{-1}$ in order to maximize the reliability of a coin cell because there is much useless volume adsorbing the electrolyte compared with a pouch cell.[50] Moreover, LiNO$_3$ as a well-known additive was employed to enhance the performance of Li–S batteries. The performance of Li–S batteries under mild conditions was significantly improved (Figure S14).

In particular, under practical conditions, Li–S batteries maintain stable within 120 cycles in EPSE and 62 cycles in PSE when capacity retention reaches 60% (Figure 6a). The specific capacity and CE at the 5th cycle are 909 mAh g^{-1} and

Figure 5. Electrochemical performance of LiNO$_3$-free electrolyte in Li–S batteries under mild conditions. a) Cycling performance and CE of Li–S batteries with PSE and EPSE electrolytes at 0.1 C. b) Shuttle current versus applied potentiostatic charging voltage. The morphology of deposited Li after 5 cycles in c) PSE and d) EPSE. e) XPS spectra of S 2p on the surface of Li at the 5th cycle in EPSE (left) and PSE (middle) after 0- and 5-min sputtering. The right panel is the evolution of the atomic concentration of S with sputtering time.
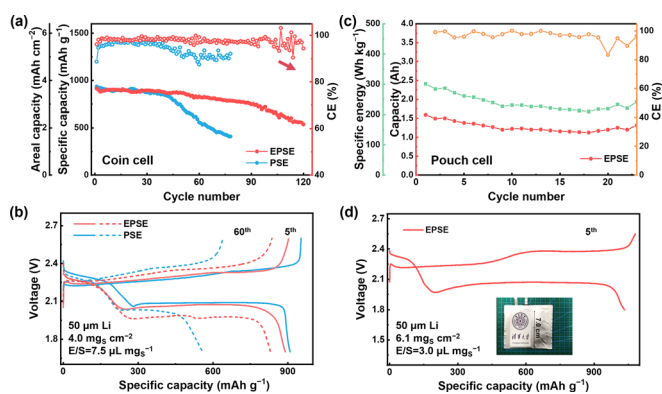
Figure 6. Cycling performance of various electrolytes with LiNO$_3$ additives in Li–S batteries under practical conditions. a) The performance of Li–S batteries under practical conditions and b) the corresponding voltage–specific capacity profiles at the 5th and 60th cycle at 0.1 C. c) Cycling performance of a Li–S pouch cell and the corresponding voltage–specific capacity at the 5th cycle at 0.025 C. The detailed test conditions and optical image of the pouch cell are inset in (b) and (d), respectively.

■■■■
↖↙ **These are not the final page numbers!**

www.angewandte.org

© 2021 Wiley-VCH GmbH

Angew. Chem. Int. Ed. **2021**, *60*, 2 – 9

95.5 % in PSE, and 889 mAh g^{-1} and 98.5 % in EPSE (Figure 6b). The slightly decreased specific capacity in EPSE results from the decreased capacity of the first plateau. The dissolution of PSs in EPSE is limited due to the introduction of DIPE. The theoretical concentration of PSs required to be dissolved at E/S ratio of 7.5 µL mg$_S^{-1}$ is 0.50 M Li$_2$S$_8$, which is beyond the limitation of EPSE (ca. 0.20 M Li$_2$S$_8$) but near the limitation of PSE (0.50 M Li$_2$S$_8$). Thus, the kinetical performance and the specific capacity at the first plateau slightly decrease because the first plateau is a solution-mediated process which is sensitive to the dissolution of PSs. Still, the kinetic performance of S cathode under practical conditions in EPSE is also competitive with PSE and significantly outperforms sparingly solvating electrolyte. After 45 cycles, specific capacity and CE fade more rapidly than before in PSE due to the consumption of fresh Li (Figure S15). However, the knee point with EPSE is significantly delayed to the 90th cycle. Then, a slower decay is in EPSE than PSE after the knee point. Furthermore, uniform and uncorroded morphology of Li deposition after cycles is also achieved in EPSE under practical conditions (Figure S16). Although the full dissolution of PSs is much difficult in EPSE, the encapsulation of partial dissolved PSs still functions. Consequently, the parasitic reactions are well mitigated and Li metal anode is stabilized in EPSE according to the double lifespan under practical conditions.

Pouch cells were further assembled to explore the potential of EPSE in practical. A pouch cell (1.6 Ah) with ultrathin Li anodes (50 µm), lean electrolytes (3.0 µL mg$_S^{-1}$), and high loading S cathodes (6.1 mg$_S$ cm^{-2}) was employed, which is harsher than a coin cell. The specific energy of the pouch cell is 300 Wh kg^{-1} including the mass of the all components of a pouch cell (Figure 6c, S17).[13] The pouch cell can maintain capacity retention of 81 % with an average CE of 96.4 % after 23 cycles (Figure S18). The specific capacity of the 1st cycle is 1172 mAh g^{-1} (Figure 6d). Although the discharge polarization voltage inevitably increases by 60 mV due to sharply increased concentration of PSs (0.75 M Li$_2$S$_8$ in practical) and large viscosity of electrolyte as expected, it is comparable with the normal performance of PSE,[32,51] ensuring high energy density of a pouch cell. Therefore, it is concluded that the introduction of encapsulated PSs in EPSE significantly enhances the lifespan and CE of Li–S batteries under practical conditions even at the pouch cell level.

Conclusion

The electrolyte structure of PSs, that is the two solvent shells around PSs, was unveiled by the combinations of molecular dynamics simulations and experimental measurements. The reduction resistance of the solvent shells plays a vital role in decreasing the reactivity of PSs against Li metal. By the molecular-scale regulation, PSs can be encapsulated into anti-reductive solvent shells in order to decrease the reactivity of PSs. While employing an electrolyte with DIPE as a cosolvent, DIPE molecules tend to distribute in the outer solvent shell around PSs. DIPE molecule has a higher stability than conventional ether solvents and thus the reduction

resistance of the outer shell against Li metal is improved, obstructing the parasitic reactions. Furthermore, the dissolution of PSs is ensured by the conventional ether solvents in the inner shell, which maintains the satisfying kinetic performance of S cathode. When it comes to practical conditions with a limited Li anode (50 µm), a high loading S cathode (4.0 mg$_S$ cm^{-2}), and a low E/S ratio (7.5 µL mg$_S^{-1}$), the lifespan of Li–S batteries increased from 62 to 120 cycles. A pouch cell (1.6 Ah) with a specific energy of 300 Wh kg^{-1} delivered stable cycling within 23 cycles. The fundamental understanding in this work provides a fresh ground to understand the electrolyte structure of PSs and the rational electrolyte design in Li–S and analogous batteries in which the reaction intermediates of electrode are reactive and dissolved into electrolytes.

Conflict of interest

The authors declare no conflict of interest.

Keywords: electrolyte structure · lithium metal anode · lithium–sulfur batteries · polysulfide encapsulation · solvent shell

[1] S. Chu, Y. Cui, N. Liu, *Nat. Mater.* **2017**, *16*, 16.
[2] M. Marinaro, D. Bresser, E. Beyer, P. Faguy, K. Hosoi, H. Li, J. Sakovica, K. Amine, M. Wohlfahrt-Mehrens, S. Passerini, *J. Power Sources* **2020**, *459*, 228073.
[3] D. Lin, Y. Liu, Y. Cui, *Nat. Nanotechnol.* **2017**, *12*, 194.
[4] A. Manthiram, Y. Fu, S. H. Chung, C. Zu, Y. S. Su, *Chem. Rev.* **2014**, *114*, 11751.
[5] M. Hagen, D. Hanselmann, K. Ahlbrecht, R. Maca, D. Gerber, J. Tubke, *Adv. Energy Mater.* **2015**, *5*, 1401986.
[6] A. Gupta, A. Bhargav, A. Manthiram, *Adv. Energy Mater.* **2019**, *9*, 1803096.
[7] S. S. Zhang, *J. Power Sources* **2013**, *231*, 153.
[8] C. Shen, J. Xie, M. Zhang, P. Andrei, M. Hendrickson, E. J. Plichta, J. P. Zheng, *Electrochim. Acta* **2017**, *248*, 90.
[9] S. Drvarič Talian, G. Kapun, J. Moškon, A. Vizintin, A. Randon-Vitanova, R. Dominko, M. Gaberšček, *Chem. Mater.* **2019**, *31*, 9012.
[10] S. H. Chung, A. Manthiram, *Adv. Mater.* **2019**, *31*, 1901125.
[11] M. Zhao, B. Q. Li, X. Q. Zhang, J. Q. Huang, Q. Zhang, *ACS Cent. Sci.* **2020**, *6*, 1095.

Angew. Chem. Int. Ed. **2021**, *60*, 2–9

© 2021 Wiley-VCH GmbH

www.angewandte.org

These are not the final page numbers!

[12] X. B. Cheng, C. Yan, J. Q. Huang, P. Li, L. Zhu, L. D. Zhao, Y. Y. Zhang, W. C. Zhu, S. T. Yang, Q. Zhang, *Energy Storage Mater.* **2017**, *6*, 18.

[13] L. L. Shi, S. M. Bak, Z. Shadike, C. Q. Wang, C. J. Niu, P. Northrup, H. K. Lee, A. Y. Baranovskiy, C. S. Anderson, J. Qin, S. Feng, X. D. Ren, D. Y. Liu, X. Q. Yang, F. Gao, D. P. Lu, J. Xiao, J. Liu, *Energy Environ. Sci.* **2020**, *13*, 3620.

[14] W. Xu, J. L. Wang, F. Ding, X. L. Chen, E. Nasybutin, Y. H. Zhang, J. G. Zhang, *Energy Environ. Sci.* **2014**, *7*, 513.

[15] X. Ji, K. T. Lee, L. F. Nazar, *Nat. Mater.* **2009**, *8*, 500.

[16] S. Xin, L. Gu, N. H. Zhao, Y. X. Yin, L. J. Zhou, Y. G. Guo, L. J. Wan, *J. Am. Chem. Soc.* **2012**, *134*, 18510.

[17] B. Q. Li, S. Y. Zhang, L. Kong, H. J. Peng, Q. Zhang, *Adv. Mater.* **2018**, *30*, 1707483.

[18] Y. S. Su, A. Manthiram, *Chem. Commun.* **2012**, *48*, 8817.

[19] M. Zhao, H. J. Peng, Z. W. Zhang, B. Q. Li, X. Chen, J. Xie, X. Chen, J. Y. Wei, Q. Zhang, J. Q. Huang, *Angew. Chem. Int. Ed.* **2019**, *58*, 3779; *Angew. Chem.* **2019**, *131*, 3819.

[20] T. F. Liu, H. L. Hu, X. F. Ding, H. D. Yuan, C. B. Jin, J. W. Nai, Y. J. Liu, Y. Wang, Y. H. Wan, X. Y. Tao, *Energy Storage Mater.* **2020**, *30*, 346.

[21] B. Q. Li, H. J. Peng, X. Chen, S. Y. Zhang, J. Xie, C. X. Zhao, Q. Zhang, *CCS Chem.* **2019**, *1*, 128.

[22] Q. Pang, X. Liang, C. Y. Kwok, L. F. Nazar, *Nat. Energy* **2016**, *1*, 16132.

[23] M. R. Kaiser, S. Chou, H. K. Liu, S. X. Dou, C. Wang, J. Wang, *Adv. Mater.* **2017**, *29*, 1700449.

[24] S. Xiong, M. Regula, D. Wang, J. Song, *Electrochem. Energy Rev.* **2018**, *1*, 388.

[25] L. Cheng, L. A. Curtiss, K. R. Zavadil, A. A. Gewirth, Y. Y. Shao, K. G. Gallagher, *ACS Energy Lett.* **2016**, *1*, 503.

[26] K. Ueno, J. W. Park, A. Yamazaki, T. Mandai, N. Tachikawa, K. Dokko, M. Watanabe, *J. Phys. Chem. C* **2013**, *117*, 20509.

[27] L. Suo, Y. S. Hu, H. Li, M. Armand, L. Chen, *Nat. Commun.* **2013**, *4*, 1481.

[28] M. Cuisinier, P. E. Cabelguen, B. D. Adams, A. Garsuch, M. Balasubramanian, L. F. Nazar, *Energy Environ. Sci.* **2014**, *7*, 2697.

[29] K. Sun, Q. Wu, X. Tong, H. Gan, *ACS Appl. Energy Mater.* **2018**, *1*, 2608.

[30] K. Dokko, N. Tachikawa, K. Yamauchi, M. Tsuchiya, A. Yamazaki, E. Takashima, J. W. Park, K. Ueno, S. Seki, N. Serizawa, M. Watanabe, *J. Electrochem. Soc.* **2013**, *160*, A1304.

[31] Q. Pang, A. Shyamsunder, B. Narayanan, C. Y. Kwok, L. A. Curtiss, L. F. Nazar, *Nat. Energy* **2018**, *3*, 783.

[32] C. Weller, S. Thieme, P. Härtel, H. Althues, S. Kaskel, *J. Electrochem. Soc.* **2017**, *164*, A3766.

[33] S. Dörfler, S. Walus, J. Locke, A. Fotouhi, D. J. Auger, N. Shateri, T. Abendroth, P. Härtel, H. Althues, S. Kaskel, *Energy Technol.* **2021**, *9*, 2000694.

[34] K. S. Han, J. Chen, R. Cao, N. N. Rajput, V. Murugesan, L. Shi, H. Pan, J.-G. Zhang, J. Liu, K. A. Persson, K. T. Mueller, *Chem. Mater.* **2017**, *29*, 9023.

[35] C. Park, A. Ronneburg, S. Risse, M. Ballauff, M. Kanduč, J. Dzubiella, *J. Phys. Chem. C* **2019**, *123*, 10167.

[36] K. H. Wujcik, T. A. Pascal, C. D. Pemmaraju, D. Devaux, W. C. Stolte, N. P. Balsara, D. Prendergast, *Adv. Energy Mater.* **2015**, *5*, 1500285.

[37] X. Bogle, R. Vazquez, S. Greenbaum, A. Cresce, K. Xu, *J. Phys. Chem. Lett.* **2013**, *4*, 1664.

[38] M. Li, C. Wang, Z. Chen, K. Xu, J. Lu, *Chem. Rev.* **2020**, *120*, 6783.

[39] C. C. Su, M. He, R. Amine, Z. Chen, K. Amine, *Angew. Chem. Int. Ed.* **2018**, *57*, 12033; *Angew. Chem.* **2018**, *130*, 12209.

[40] X. Deng, M. Y. Hu, X. Wei, W. Wang, Z. Chen, J. Liu, J. Z. Hu, *J. Power Sources* **2015**, *285*, 146.

[41] I. P. Gerothanassis, *Prog. Nucl. Magn. Reson. Spectrosc.* **2010**, *56*, 95.

[42] M. T. Béraldin, E. Vauthier, S. Fliszár, *Can. J. Chem.* **1982**, *60*, 106.

[43] X. Ren, L. Zou, X. Cao, M. H. Engelhard, W. Liu, S. D. Burton, H. Lee, C. Niu, B. E. Matthews, Z. Zhu, C. Wang, B. W. Arey, J. Xiao, J. Liu, J.-G. Zhang, W. Xu, *Joule* **2019**, *3*, 1662.

[44] G. Li, Q. Huang, X. He, Y. Gao, D. Wang, S. H. Kim, D. Wang, *ACS Nano* **2018**, *12*, 1500.

[45] M. T. Lee, H. D. Liu, D. Brandell, *Batteries Supercaps* **2020**, *3*, 1370.

[46] F. Y. Fan, Y. M. Chiang, *J. Electrochem. Soc.* **2017**, *164*, A917.

[47] D. Aurbach, E. Pollak, R. Elazari, G. Salitra, C. S. Kelley, J. Affinito, *J. Electrochem. Soc.* **2009**, *156*, A694.

[48] S. Z. Xiong, K. Xie, Y. Diao, X. B. Hong, *J. Power Sources* **2014**, *246*, 840.

[49] A. Bhargav, J. R. He, A. Gupta, A. Manthiram, *Joule* **2020**, *4*, 285.

[50] X. Q. Zhang, T. Li, B. Q. Li, R. Zhang, P. Shi, C. Yan, J. Q. Huang, Q. Zhang, *Angew. Chem. Int. Ed.* **2020**, *59*, 3252; *Angew. Chem.* **2020**, *132*, 3278.

[51] X. Y. Huang, J. J. Xue, M. Xiao, S. J. Wang, Y. N. Li, S. C. Zhang, Y. Z. Meng, *Energy Storage Mater.* **2020**, *30*, 87.
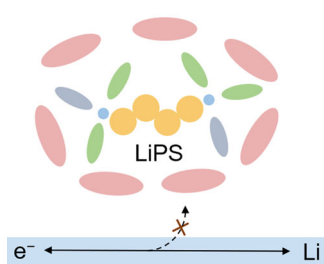
Research Articles

Electrochemistry

X.-Q. Zhang, Q. Jin, Y.-L. Nan, L.-P. Hou,
B.-Q. Li, X. Chen, Z.-H. Jin, X.-T. Zhang,
J.-Q. Huang, Q. Zhang* —— ▮▮▮▮–▮▮▮▮

Electrolyte Structure of Lithium
Polysulfides with Anti-Reductive Solvent
Shells for Practical Lithium–Sulfur
Batteries

Li–S batteries

The electrolyte structure of lithium poly-
sulfides (PSs) with anti-reductive solvent
shells was unveiled. The reduction
resistance of the solvent shell is proven to
be a key reason for the decreased reac-
tivity of PSs towards Li. With isopropyl
ether as a cosolvent, the reactivity of PSs
is suppressed by encapsulating PSs into
anti-reductive solvent shells. The stability
of practical Li–S batteries was improved
and a pouch cell of 300 Wh kg^{-1} was
demonstrated.